Journal of Vacuum Science & Technology A

PLEASE CITE THIS ARTICLE AS DOI: 10.1116/6.0003457

Effect of Background Gas Composition on the Stoichiometry and Lithium Ion Conductivity of Pulse Laser Deposited Epitaxial Lithium Lanthanum Tantalate ($Li_{3x}La_{1/3-x}TaO_3$)

Ian A. Brummel[1, a)], Chuanzhen Zhou[2], and Jon F. Ihlefeld[1,3, a)]

[1]Department of Materials Science and Engineering, University of Virginia, Charlottesville, Virginia 22904 (USA)
[2]Analytical Instrumentation Facility, North Carolina State University, Raleigh, North Carolina 27695 (USA)
[3]Department of Electrical and Computer Engineering, University of Virginia, Charlottesville, Virginia 22904 (USA)

[a)] Electronic mail: iab5dy@virginia.edu, jfi4n@virginia.edu.

Lithium lanthanum tantalate ($Li_{3x}La_{1/3-x}TaO_3$, $x = 0.075$) thin films are grown via pulsed laser deposition using background gas atmospheres with varying partial pressures of oxygen and argon. The background gas composition was varied from 100% to 6.6% oxygen with the pressure fixed at 150 mTorr. The maximum ion conductivity of 1.5×10^{-6} S/cm was found for the film deposited in 100% oxygen. The ion conductivity of the films was found to decrease with reduced oxygen content from 100% to 16.6% O_2 in the background gas. The 6.6% oxygen background condition produced ion conductivity that approached that of the 100% oxygen condition film. The lithium transfer from the target to the film was found to decrease monotonically with decreasing oxygen content in the background gas but did not account for all changes in the ion conductivity. The activation energy of ion conduction was measured and found to correlate well with the measured ion conductivity trends. Analysis of X-ray diffraction results revealed that the films also exhibited a change in the lattice parameter that directly correlated with the ion conduction activation energy, indicating that a primary factor for determining the conductivity of these films is the changing size of the ion conduction bottleneck, which controls the activation energy of ion conduction.

Journal of Vacuum Science & Technology A

PLEASE CITE THIS ARTICLE AS DOI: 10.1116/6.0003457

I. INTRODUCTION

Solid state ion conductors are a promising component toward improving the safety and energy density of lithium ion battery technology. Electrolytes composed of these materials may enable the use of higher energy electrode materials because they exhibit wide practical electrochemical stability windows as a result of the formation of solid electrolyte interlayers that passivate the electrode-electrolyte contact.[1–3] The mechanical and thermal stability of solid state lithium ion conductors can also confer benefits in the form of safety, by reducing the likelihood of dendrite formation or thermal runaway events.[4] Finally, solid state ion conductors, particularly those that are oxides, are rarely highly reactive to air or other chemicals, eliminating the explosive failure mode of liquid electrolyte lithium ion batteries that can cause property damage or the loss of lives.[5–7] Solid state electrolytes commonly comprise a single, dense layer in order to serve as both a separator and the ion conduction medium in a battery. This calls importance to understanding the fundamental properties of the materials. For instance, understanding the anisotropy of ion conduction could be important for layers with a textured microstructure. To best understand the fundamental mechanisms of ion conduction in solid electrolyte materials, measurements of single-crystalline materials would be desirable. In many cases, however, single crystalline specimens of materials of interest are not available commercially, are challenging to prepare in sizes amenable to characterization, or they are prohibitively expensive. Epitaxial depositions of these materials can fill these gaps by enabling the measurement of single crystalline materials prepared via commonly available vapor deposition techniques, such as pulsed laser deposition (PLD).

Much of the historical PLD literature cites the technique as providing stoichiometric transfer of materials from the target to the substrate.[8] While this appears approximately true when working with materials that are composed of atoms with similar atomic masses,[9–11] there has been more recent work that shows with large variation in cation mass, the composition in the film can deviate from that of the target by up to 70%.[12–14] Other experiments have revealed that lithium transfer from the target to the

Journal of Vacuum Science & Technology A

PLEASE CITE THIS ARTICLE AS DOI: 10.1116/6.0003457

substrate is significantly less than unity, requiring accommodation to generate films with the desired composition.[15] Several aspects of the PLD parameter space have been investigated for their effects on the transfer ratios of different cations, revealing that there is a complicated interplay of factors that determines the final film composition.[11,13,14,16,17] While the total background gas pressure has been investigated for composition control, the effect of varied background gas composition on cation transfer during PLD is a notable knowledge gap.

In this work, the *A*-site deficient perovskite, $Li_{3x}La_{1/3-x}TaO_3$ (LLTaO) is used as a model system for studying single crystalline ion conductivity behavior as a function of the variation of the background gas composition during epitaxial PLD. LLTaO is chosen as a model system because it shares the *A*-site deficient perovskite structure of the well-studied lithium ion conducting system $Li_{3x}La_{2/3-x}TiO_3$. However, for some compositions of LLTaO (e.g. $x \geq 0.075$) the material adopts a cubic symmetry, eliminating the need to account for the effects of twin boundaries when measuring epitaxial film properties.[18–20] Additionally, LLTaO has a lattice parameter of ~3.94 Å, which makes it amenable to epitaxial growth on widely available cubic $SrTiO_3$ substrates with less than 1.5% lattice mismatch strain.[21,22] While LLTaO exhibits lower lithium ion conductivity than that of the closely related titanate, due to the valence-stable tantalum ion on the *B*-site, it should not be as susceptible to reactions with high energy electrodes such as lithium metal and may be better suited for secondary battery applications.[18]

II. EXPERIMENTAL

Epitaxial thin films with the nominal composition of $Li_{3x}La_{1/3-x}TaO_3$, where $x = 0.075$, were fabricated on single crystalline (001)-oriented $SrTiO_3$ substrates (MTI Corporation, Richmond, CA, USA) using pulsed laser deposition (PLD). Depositions were conducted within a custom high-vacuum system using a target carousel and substrate heater from NBM Design (Bel Air, MD, USA), where substrates were attached to the heater platen using conductive silver paint (Ted Pella, Redding, CA, USA). All films were deposited at a substrate temperature of 700 °C ± 10 °C as measured by a Fluke

Journal of Vacuum Science & Technology A

PLEASE CITE THIS ARTICLE AS DOI: 10.1116/6.0003457

Endurance E2RL 2-color pyrometer (Everett, WA, USA) with a target-to-substrate distance of 68 mm. The total background pressure for each film growth was kept constant at 150 mTorr as measured with an MKS Instruments 627F capacitance manometer gauge (Andover, MA, USA), with varying partial pressure of oxygen and argon determined by the relative gas flow set using mass flow controllers (Alicat Scientific, Tucson, AZ, USA). Oxygen content was varied to generate pO_2 conditions of 100%, 50%, 16.6%, and 6.6%. Gas pressure and temperature were allowed to stabilize for 40 minutes prior to commencing deposition. The laser excitation voltage of the Lambda Physik COMPex 205 excimer laser (248 nm wavelength) was kept constant for each deposition and was set such that the fluence at the target surface was ~1.4 J/cm^2. Prior to deposition, the targets were exposed to 1800 laser pulses at 10 Hz to clean the target surface then 18200 pulses at 10 Hz were used to deposit the film. Targets were rastered and rotated such that the point of laser focus was not allowed to dwell in a single area to allow even usage of the target surface for deposition. Targets were fabricated using a solid state synthesis method. Precursors of Li_2CO_3 (99+%, Arcos Organics), La_2O_3 (99.9%, Alfa Aesar), and Ta_2O_5 (99.9%, TANiOBIS GmbH) were combined in stoichiometric amounts, plus 20 at.% excess lithium to account for losses during high temperature calcining and sintering treatments and in the plasma during deposition. The target synthesis procedure is detailed in previous work.[23] All targets were generated from the same parent batch of precursors and were sintered in a single furnace run. After initial characterization, the films were annealed at 950 °C for 30 minutes in flowing oxygen in a tube furnace to promote crystallinity and LLTaO phase formation.

The crystal structure of the films in an out-of-plane (2θ-ω) geometry was characterized by X-ray diffraction (XRD) using a Panalytical Empyrean diffractometer, using Cu-Kα radiation (Malvern Panalytical, Malvern, UK). The epitaxial relationship (ϕ-scans) between the film and substrate was characterized using a Rigaku Smartlab diffractometer with Cu-Kα radiation (Rigaku Corporation, Akishima-shi, Tokyo, Japan). Film cross sections were prepared by milling a trench in the film using a focused ion beam (FIB) with a gallium ion source in a Helios UC G4 Dual Beam FIB (Thermo Fisher Scientific, Waltham, MA, USA). Scanning electron microscopy (SEM) of the cross sections was then performed using beam conditions of 5 keV, 0.20 nA at an incident

Journal of Vacuum Science & Technology A

PLEASE CITE THIS ARTICLE AS DOI: 10.1116/6.0003457

angle of 56° with tilt correction and dynamic focus within the same instrument. Characterization of the lithium content in the films was carried out with secondary ion mass spectroscopy (SIMS) by the Analytical Instrumentation Facility (AIF) at North Carolina State University using a TOF SIMS V instrument (ION TOF, Inc. Chestnut Ridge, NY). 10 keV Cs^+ with 23 nA current was used to create a 120 μm × 120 μm milled area and the middle 50 μm by 50 μm area was analyzed using 0.35 pA Bi_3^+ primary ion beam. Depth profile data was measured, and the relative lithium content was determined by using the average counts for each species in the steady-state region of the depth profiles. This process is further described in the caption of Supplemental Figure 1, which can be found at [URL will be inserted by AIP Publishing]. Platinum electrodes were deposited by DC magnetron sputtering through a custom shadow mask to produce bar-shaped electrodes with nominal dimension of 3 × 0.75 mm and nominal spacing of 0.75 mm along the conduction path. Actual electrode dimensions were measured by image analysis of optical micrographs using a stage micrometer for scale. Impedance spectroscopy data was collected between 10 MHz and 50 mHz with a 2.5 V oscillator, using a Solartron 1260A frequency response analyzer with a Solartron 1296A dielectric interface to allow for measurement of high impedance samples (Solartron Metrology, Bognor Regis, West Sussex, UK). Impedance spectroscopy measurements were carried out in an Instec vacuum probe station with a heating stage (model HP621HVF, Instec Inc., Boulder, CO, USA) where typical vacuum levels of 1×10^{-4} Torr were achieved during measurement. Impedance spectra were fit using EC-Lab software (Bio-Logic S.A.S., Claix, France) for extraction of conductivity and activation energy values.

III. RESULTS AND DISCUSSION

$Li_{3x}La_{1/3-x}TaO_3$ exhibits both a cubic and a tetragonal polymorph depending on the value of x, where the tetragonal phase is made up of a supercell of two pseudocubic perovskite cells that exhibit ordering of the lanthanum atoms on alternating $(001)_t$ planes (where the subscript t denotes tetragonal symmetry).[24] The out-of-plane XRD patterns are shown for the as-deposited films in Figure 1(A), with smaller 2θ range views of the peaks associated with $\{001\}_p$ reflections shown in Figure 1(B-E) (where the p subscript denotes

Journal of Vacuum Science & Technology A

PLEASE CITE THIS ARTICLE AS DOI: 10.1116/6.0003457

pseudo-cubic symmetry). From these patterns, it is evident that all films showed some crystallinity in their as-deposited state. The 100%, 50%, and 16.6% oxygen background films exhibit peaks that can be readily indexed to the cubic LLTaO phase and the substrate, which are indicated by the diamond and star markers, respectively. Careful observation of the spacing between the film and substrate peaks in Figure 1(B-C) reveals that there is a slight decrease in the lattice parameter of the LLTaO phase with decreased oxygen partial pressure. These patterns also display two peaks that can be indexed to the $(001)_t$ and $(003)_t$ peaks of the tetragonal phase, as indicated by triangular markers. The tetragonal peaks are of low intensity but increase in relative intensity slightly as the oxygen partial pressure in the background gas is reduced. The intensity ratio for the $(001)_t$ to $(001)_p$ peaks was found to be 0.33%, 0.49%, and 0.70% for the 100%, 50%, and 16.6% oxygen background samples, respectively. This is markedly lower than the calculated intensity ratio of 23% for the tetragonal structure, indicating a very low level of ordering in the as-deposited films. The 6.6% oxygen background film exhibits peaks on the high 2θ side of the STO substrate peaks, indicating that a significant deviation from the expected LLTaO lattice parameter exists. The peaks are also broader and of lower intensity than those observed for the films deposited with higher oxygen content background gas mixtures indicating reduced crystallinity. While the peaks in the 6.6% oxygen background film follow a trend that could be consistent with a perovskite of the same space group as the cubic LLTaO, but with a significantly smaller lattice parameter, there are not enough peaks present to positively identify this phase.

Journal of Vacuum Science & Technology A

PLEASE CITE THIS ARTICLE AS DOI: 10.1116/6.0003457

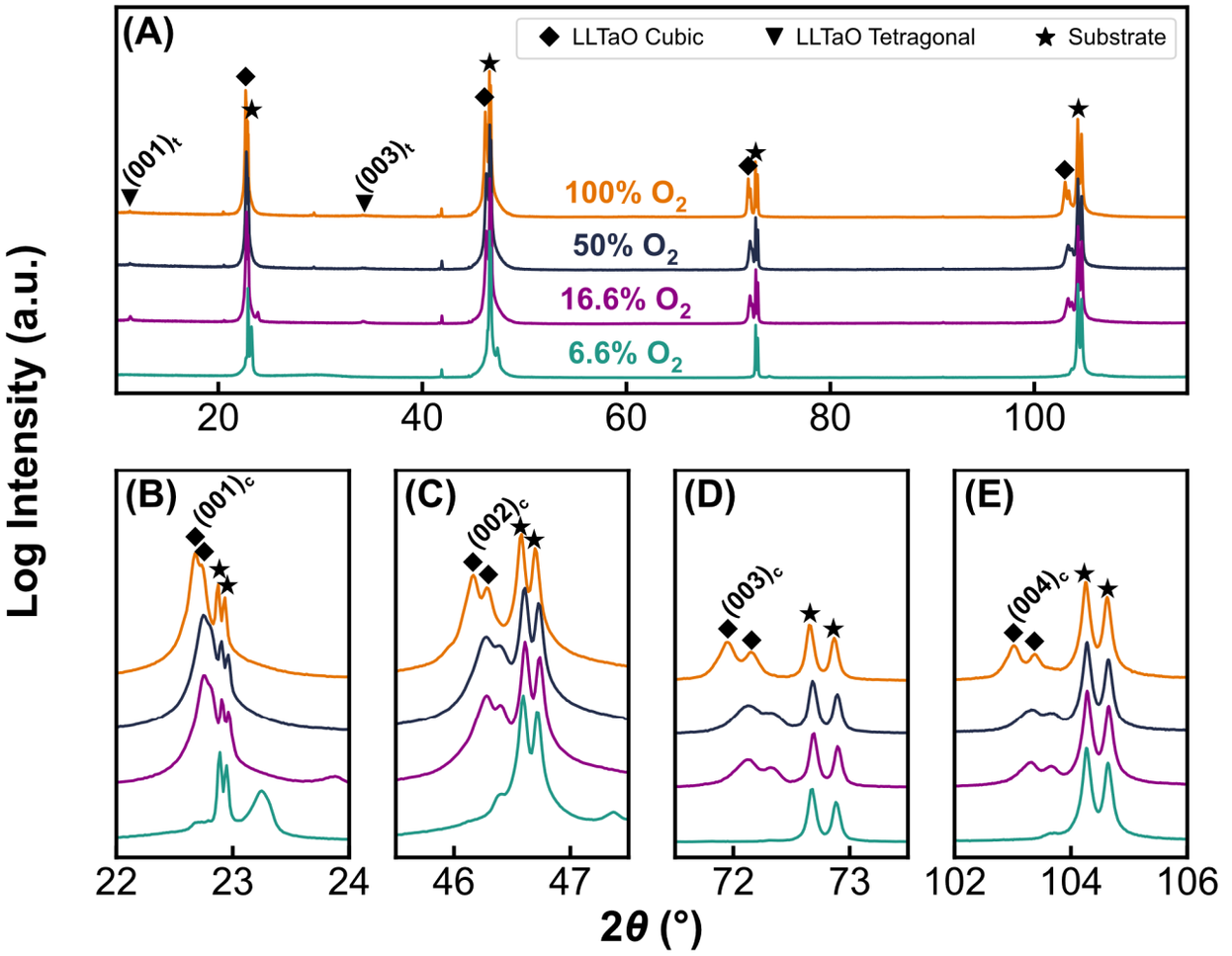

FIG. 1. Normalized X-ray diffraction patterns generated from a 2θ-ω geometry to identify the phases present in the as deposited films. The full 2θ range is shown in panel (A), with detail views of the regions surrounding the (B) $SrTiO_3$ (001), (C) $SrTiO_3$ (002), (D) $SrTiO_3$ (003), and (E) $SrTiO_3$ (004) peaks. Substrate peaks are marked with a star, psuedocubic films peaks are marked by diamonds, and tetragonal film peaks are marked by triangles.

Most of the trends that were present in the as-deposited films persist after annealing at 950 °C. Figure 2 shows an identical set of measurements to Figure 1, taken after the films had been annealed. The most notable change is the complete conversion of the film peaks observed in the 6.6% oxygen background film from the unidentified phase to the LLTaO phase. The loss of definition of the $K\alpha_1$ and $K\alpha_2$ peaks for the 6.6% oxygen background film in Figure 2(B) indicates that the film has a poorer crystal quality than

Journal of Vacuum Science & Technology A

PLEASE CITE THIS ARTICLE AS DOI: 10.1116/6.0003457

that of the films deposited with higher oxygen partial pressures. The $(001)_t$ to $(001)_p$ intensity ratio remained constant after annealing for the 100%, 50%, and 16.6% oxygen background films. With the conversion of the 6.6% oxygen background film to the LLTaO phase, the $(001)_t$ to $(001)_p$ intensity ratio can now be measured and was found to be 6.6%. This indicates that films deposited with lower oxygen contents have increased cation ordering leading to the formation of the tetragonal phase. Based on the results of Mizumoto and Hayashi, where they found that the tetragonal phase of LLTaO formed for $x < 0.075$,[24] this trend points toward a reduction in lithium transfer from the target to the films with decreased oxygen partial pressure. Finally, the trend of decreased lattice parameter with decreasing oxygen partial pressure remains the same for the 100%, 50%, and 16.6% oxygen background films, but the 6.6% oxygen background film exhibits a lattice parameter that is similar to the 100% oxygen background film. The planar spacing was calculated from each of the (002), (003), and (004) planes with displacement correction based on the STO peak positions. The lattice parameters were found to be 3.933 Å, 3.930 Å, 3.922 Å, and 3.937 Å for the 100%, 50%, 16.6%, and 6.6% oxygen background films, respectively.

Figure 3 shows the XRD scans of the (103) planes in the ϕ-axis to illustrate the epitaxial relationship between the substrate and film. Measurements were performed at $\chi = 18.435°$, with $2\theta = 77.28°$ for the (103) substrate peaks and $2\theta = 76.55°$ for the (103) film peaks. The scans show strong agreement of the substrate and film peak positions in ϕ. In combination with the data shown in Figure 2, this indicates cube-on-cube epitaxy of the LLTaO film on the STO substrate. The peaks in Figure 3 also display splitting that generally agrees between the film and substrate peaks, indicating that the starting substrates had some degree of mosaicity, which was templated into the growth of the films.

Journal of Vacuum Science & Technology A

PLEASE CITE THIS ARTICLE AS DOI: 10.1116/6.0003457

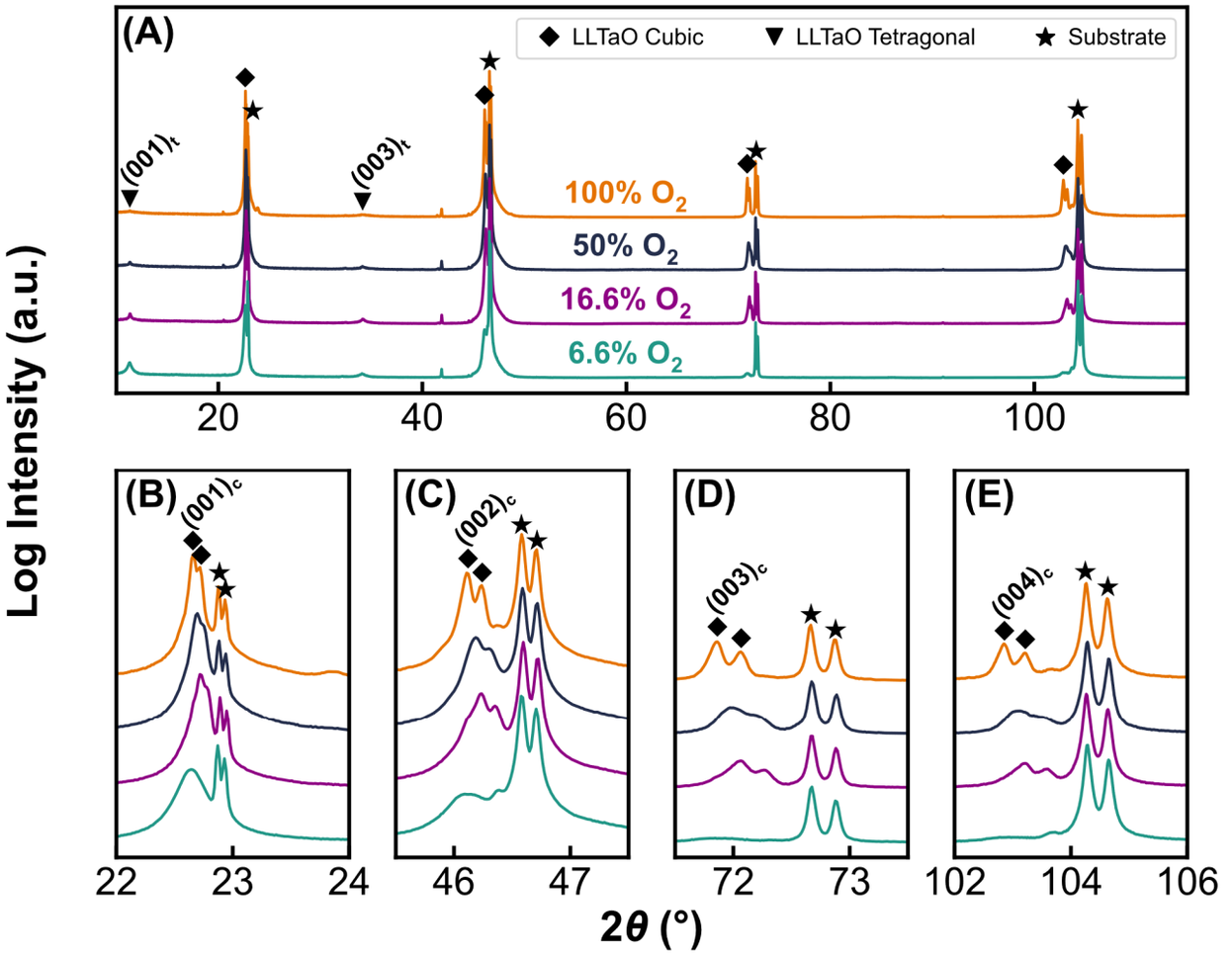

FIG. 2. Normalized X-ray diffraction patterns generated from a 2θ-ω geometry to identify the phases present in the annealed films. The full 2θ range is shown in panel (A), with detail views of the regions surrounding the (B) $SrTiO_3$ (001), (C) $SrTiO_3$ (002), (D) $SrTiO_3$ (003), and (E) $SrTiO_3$ (004) peaks. Substrate peaks are marked with a star, psuedocubic films peaks are marked by diamonds, and tetragonal film peaks are marked by triangles.

Journal of Vacuum Science & Technology A

PLEASE CITE THIS ARTICLE AS DOI: 10.1116/6.0003457

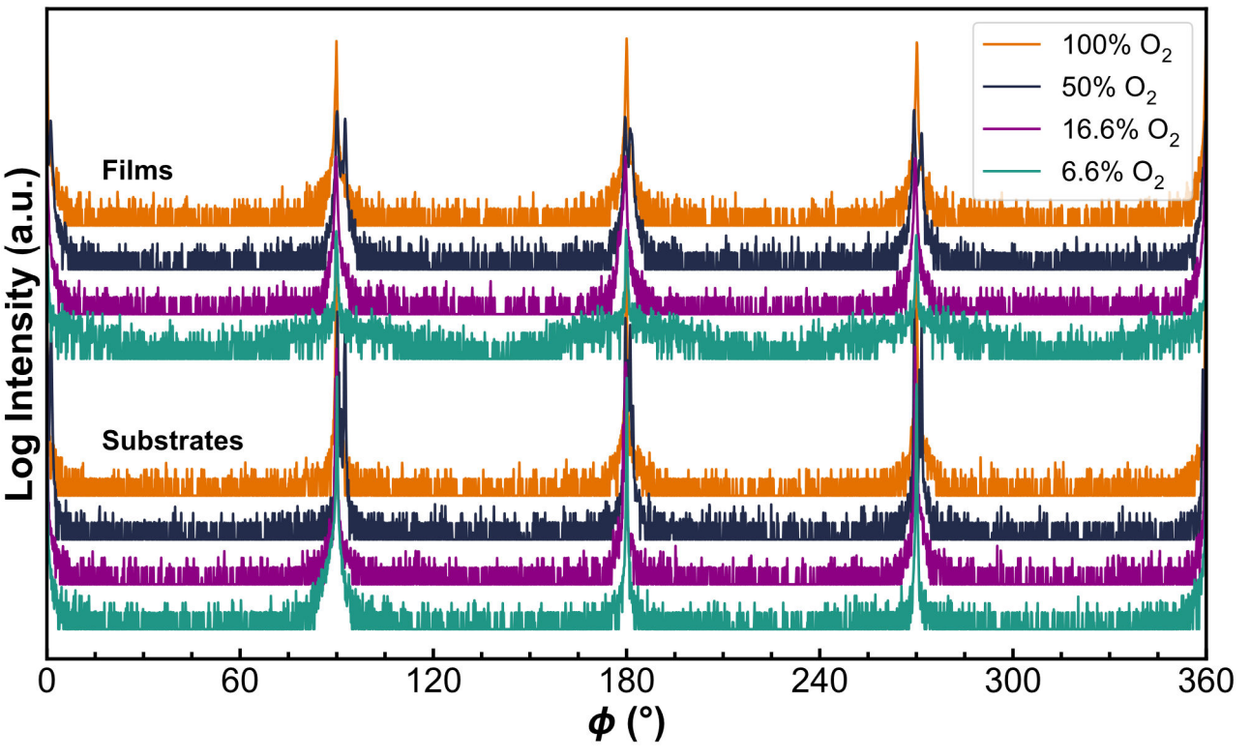

FIG. 3. ϕ-scans of the LLTaO (103) and STO (103) peaks illustrating cube-on-cube epitaxy. Multiple peaks are present in some scans as a result of mosaicity in the substrates, which was templated into the film.

Representative scanning secondary electron microscopy cross sections produced by milling a channel in the films with a gallium ion beam are shown in Figure 4. During milling the film surface was protected using two layers of platinum, the first deposited using the electron beam and the second deposited using the ion beam. The thickness of the platinum protection layers varies from sample to sample due to charging during the deposition process leading to the beam position being outside of the intended area. After milling, the channels were approximately 25 µm in width. The thickness of the films was sampled at equal intervals for a total of 20 points on each film. Thickness was determined to be 362 ± 9 nm, 375 ± 3 nm, 359 ± 5nm, and 409 ± 4 nm, where the reported error is the 95% confidence interval, for the 100%, 50%, 16.6%, and 6.6% oxygen films, respectively. Qualitatively, all films appear dense with very few boulders visible. Notably, the surface of the 100% oxygen film appears significantly rougher than those of the other films which may indicate faceted growth on the surface.

Journal of Vacuum Science & Technology A

PLEASE CITE THIS ARTICLE AS DOI: 10.1116/6.0003457

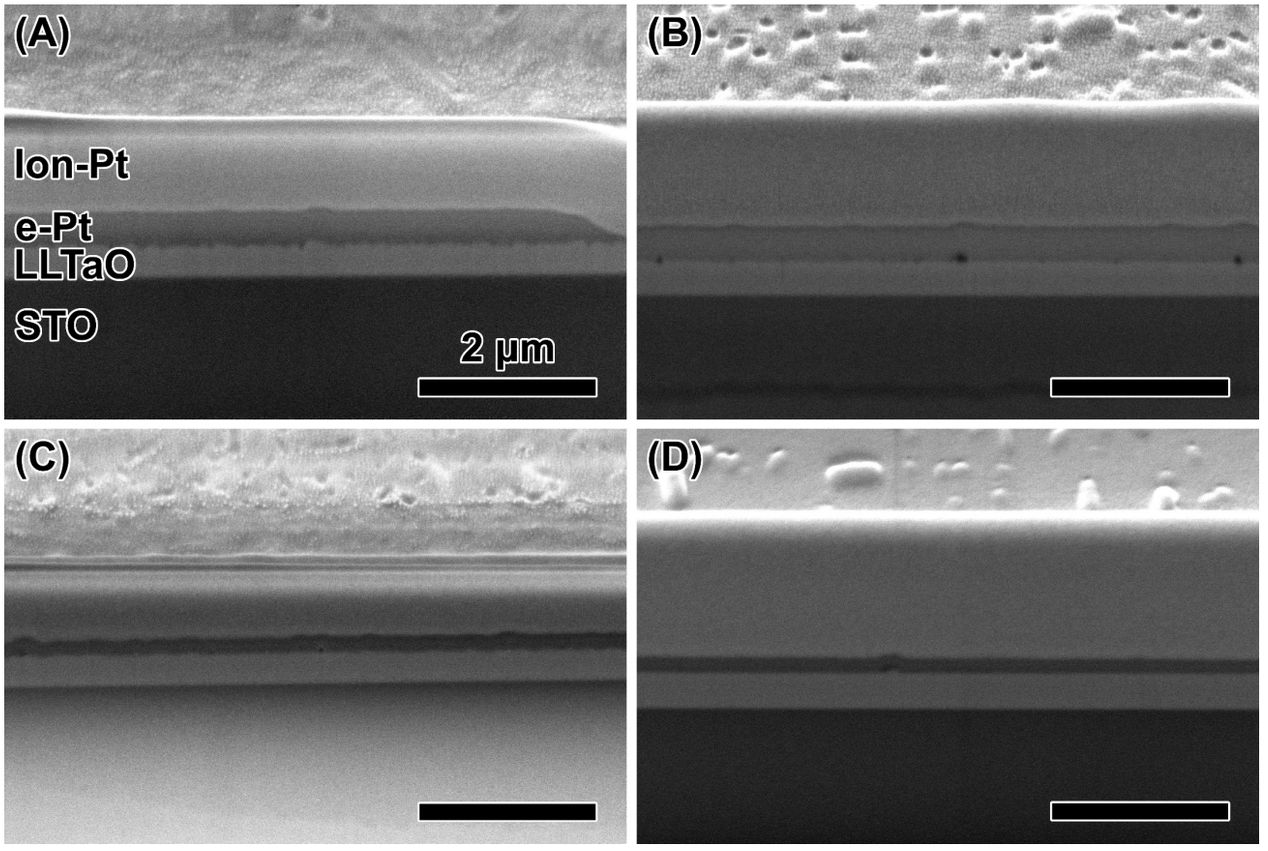

FIG. 4. Representative scanning electron micrographs of the (A) 100%, (B) 50%, (C) 16.6%, and (D) 6.6% oxygen background films after annealing. Cross sections were exposed using gallium source ion milling to cut a channel through the film and into the substrate. Films were protected using a platinum top layer that was deposited first with the electron beam then brought to thickness using ion beam deposition. A key for the visible layers is shown in panel (A).

Depth profile data from each film was collected using TOF-SIMS, with the average ratio of $CsLi^+$ to $CsTa^+$ counts shown in Figure 5 as a function of the oxygen content of the background gas. The $CsLi^+$ to $CsTa^+$ complexes were selected for measurement to suppress the contribution of matrix effects to the measurement.[25] Because there is no available standard for this material, the raw ratio of counts is presented for comparison of the amount of lithium between films. Note that this does not represent the quantitative ratio of lithium to tantalum in the films but provides a relative

Journal of Vacuum Science & Technology A

PLEASE CITE THIS ARTICLE AS DOI: 10.1116/6.0003457

measure that enables comparisons between process conditions. The lithium content decreased monotonically with decreasing oxygen content in the background gas, although the compositional difference between the 16.6% and 6.6% oxygen films was smaller than the differences found between other processing conditions. For all films, the lithium to tantalum ratio was lower than that found in a ceramic target that had not been ablated for deposition (upper solid horizontal line in the figure), with the 16.6% and 6.6% films exhibiting a lithium content lower than that of an ablated target (post-deposition, lower solid horizontal line). This indicates that while the targets are depleted of lithium during deposition, there are further losses during the transport of material from the target to the substrate, which is consistent with the formation of the tetragonal phase observed via XRD. At the relatively high deposition pressures used in this study, the mean free path of any atom in the plume is expected to be on the order of 10s of microns, which is three orders of magnitude smaller than the target to substrate distance of 68 mm. This implies that any atom that is transported from the target to the film can be expected to undergo multiple collisions with other atoms/ions in the plume or the background gas and the plume should take on diffusive characteristics.[26] See Supplemental Table I at [URL will be inserted by AIP Publishing] for calculations of the mean free path of each constituent atom. While the increased radius of argon reduces the expected mean free path, this change is on the order of a few microns. The more likely explanation for a significant decrease in the lithium transfer with decreasing oxygen (increasing argon) background is a result of the atomic mass of argon being more than double that of oxygen resulting in preferential scattering of light elements by the background gas.[26]

Journal of Vacuum Science & Technology A

PLEASE CITE THIS ARTICLE AS DOI: 10.1116/6.0003457

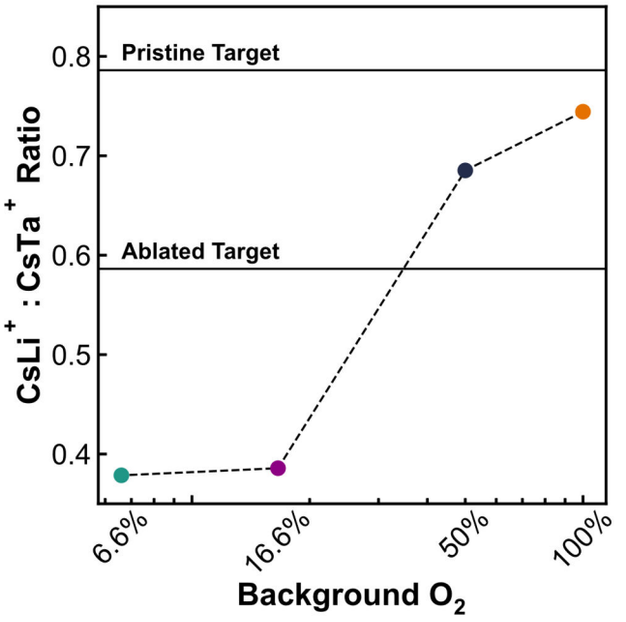

FIG. 5. Average lithium to tantalum ratio determined from TOF-SIMS depth profile measurements as a function of background oxygen during deposition. The oxygen background percentage is plotted on a log scale. Solid, horizontal lines represent the lithium to tantalum ratio found in targets prior to deposition and after the target was ablated during deposition. The dashed line between points is a guide to the eye.

An in-plane geometry, with parallel bar electrodes, was used to measure the impedance response of the LLTaO films, as represented in Figure 6(B). Representative, complex plane impedance spectra, collected at 150 °C, are shown in Figure 6(A) for each film. The data were fit using the model equivalent circuit illustrated in Figure 6(B). The circuit contains a series arrangement of one ZARC element (resistor and constant phase element in parallel) and one constant phase element representing the electrolyte and blocking electrode response, respectively. Ion conductivity was derived using Eq. (1):

$$\sigma_f = \frac{s}{RtL} \tag{1}$$

where s is the electrode spacing, t is the film thickness, L is the electrode length, and R is the resistance of the ZARC in the equivalent circuit fit. Figure 6(C) shows the extracted conductivity values of the films at room temperature. Comparison of the trend in conductivity values reveals that the reduction in lithium transfer with reduced oxygen

Journal of Vacuum Science & Technology A

content in the processing atmosphere cannot explain the entirety of the change in conductivity. Conductivity is generally represented by Eq. (2):

$$\sigma = nZ\mu \tag{2}$$

where n is the number of charge carriers, Z is the electrical charge of a carrier, and μ represents the mobility of the charge carrier. This can then be summed over all available charge carriers to give a strong approximation of the total conductivity of a material. Importantly, this implies that conductivity should be directly proportional to the number of charge carriers (lithium ion concentration) if all other elements are assumed equal. Because the conductivity of the samples deviates heavily from this assumption and the ionic charge of lithium is fixed, it can be surmised that the mobility of lithium ions is not constant with changes in the makeup of the background gas during film deposition.

Journal of Vacuum Science & Technology A

PLEASE CITE THIS ARTICLE AS DOI: 10.1116/6.0003457

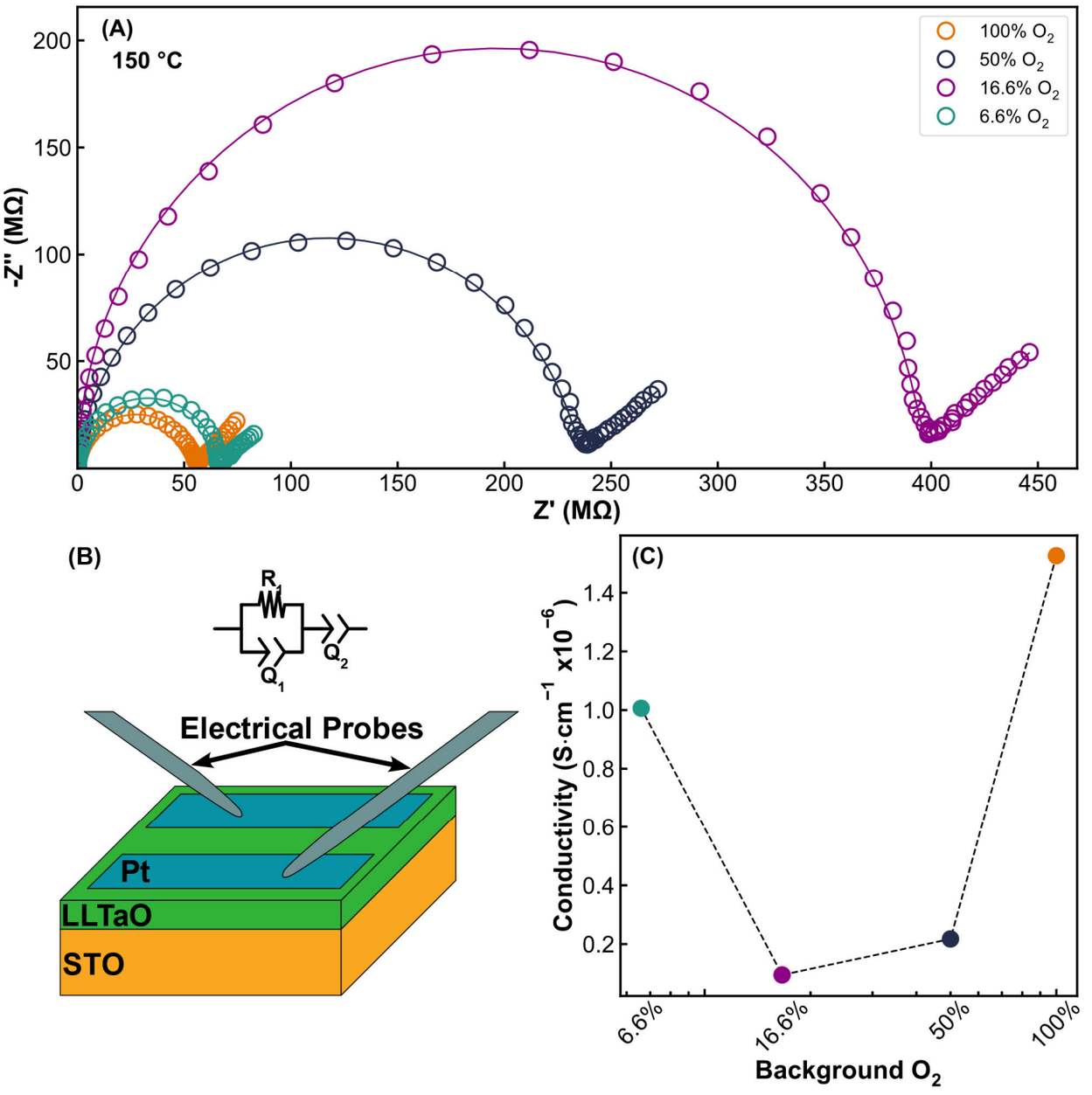

FIG. 6. (A) Complex plane impedance spectra measured at 150 °C for each film. Measured data are represented as open circles with the fit plotted as a solid line. Note that data density has been reduced to increase the legibility of the plot. (B) Schematic representations of the equivalent circuit used in fitting (top) and the electrode configuration used for in-plane impedance spectroscopy measurements (bottom) (C) Room temperature conductivity plotted as a function of the log of the oxygen content in the background gas.

Journal of Vacuum Science & Technology A

The diffusion coefficient equation:

$$D=D_0 e^{-E_a/kT} \tag{3}$$

can be combined with the Einstein relationship to reveal that the activation energy is related to the mobility of lithium in an ion conducting material as follows:

$$\mu=\frac{D}{kT} \rightarrow \mu=\frac{D_0 e^{-E_a/kT}}{kT} \tag{4}$$

where μ is the mobility, D is the diffusion coefficient, D_0 is an exponential pre-factor, E_a is the activation energy discussed above, k is Boltzmann's constant, and T is the absolute temperature. Incorporation of the Nernst-Einstein relationship allows for the development of an Arrhenius-type relationship between conductivity and activation energy via Eq. (5):

$$\sigma T=\sigma_0 e^{-E_a/kT} \rightarrow \ln(\sigma T)=-\frac{E_a}{k}*\frac{1}{T}+\ln(\sigma_0) \tag{5}$$

where σ is the ion conductivity and σ_0 is a material-dependent pre-factor. Thus, the activation energy can be calculated in a straightforward manner from the slope of a linear regression between σT and T^{-1} and can provide insight into conducting species mobility.[27,28] Impedance spectroscopy was measured at a range of temperatures from 25 to 300 °C to allow the extraction of the activation energy for ion conduction. Representative complex plane impedance spectra measured on the 100% oxygen background film are shown in Figure 7(A) to illustrate the change in impedance with increasing temperature. The analysis of conductivity, described above, was carried out at each temperature, yielding the Arrhenius-type plot shown in Figure 7(B). The activation energy was determined to be 0.41, 0.45, 0.49, and 0.43 eV for the 100%, 50%, 16.6%, and 6.6% oxygen background films, respectively. Publications investigating the bulk properties of LLTaO have shown similar values for the bulk activation energy.[19,20,29]

The qualitative trend seen for the activation energy closely matches with the inverse of the conductivity. The ion conductivity was observed to change by more than an order of magnitude as the background oxygen content was varied, while the $CsLi^+$:$CsTa^+$ ratio only changed by a factor of ~2. Additionally, the films exhibiting the highest ion conductivity (100% and 6.6% O_2) represent both the maximum and minimum

Journal of Vacuum Science & Technology A

PLEASE CITE THIS ARTICLE AS DOI: 10.1116/6.0003457

values of the $CsLi^+$:$CsTa^+$ ratio. This implies that the lithium ion mobility, as represented by measurement of the activation energy, is the dominant factor in determining the conductivity. This is further evidenced by comparing the pre-factor (σ_0) values from the Arrhenius analysis, which had a maximum difference of ~7.5% from one film to another, ruling out large changes in other parts of the ion conduction process. The activation energy for ion conduction is commonly correlated with the structural bottleneck, which must be the correct size to minimize the energy necessary for the conducting ion to move from one position to another.[19,28,30] The analysis of diffraction peak positions from Figure 2 indicates that the activation energy for lithium conduction in LLTaO is inversely correlated to the lattice parameter, with the 100% and 6.6% oxygen background films having larger lattice parameters than the other films and therefore having lower activation energy and higher ion conductivity. A similar result has been observed for bulk LLTaO where a decrease in the lattice parameter caused a significant increase in the activation energy.[23]

Journal of Vacuum Science & Technology A

PLEASE CITE THIS ARTICLE AS DOI: 10.1116/6.0003457

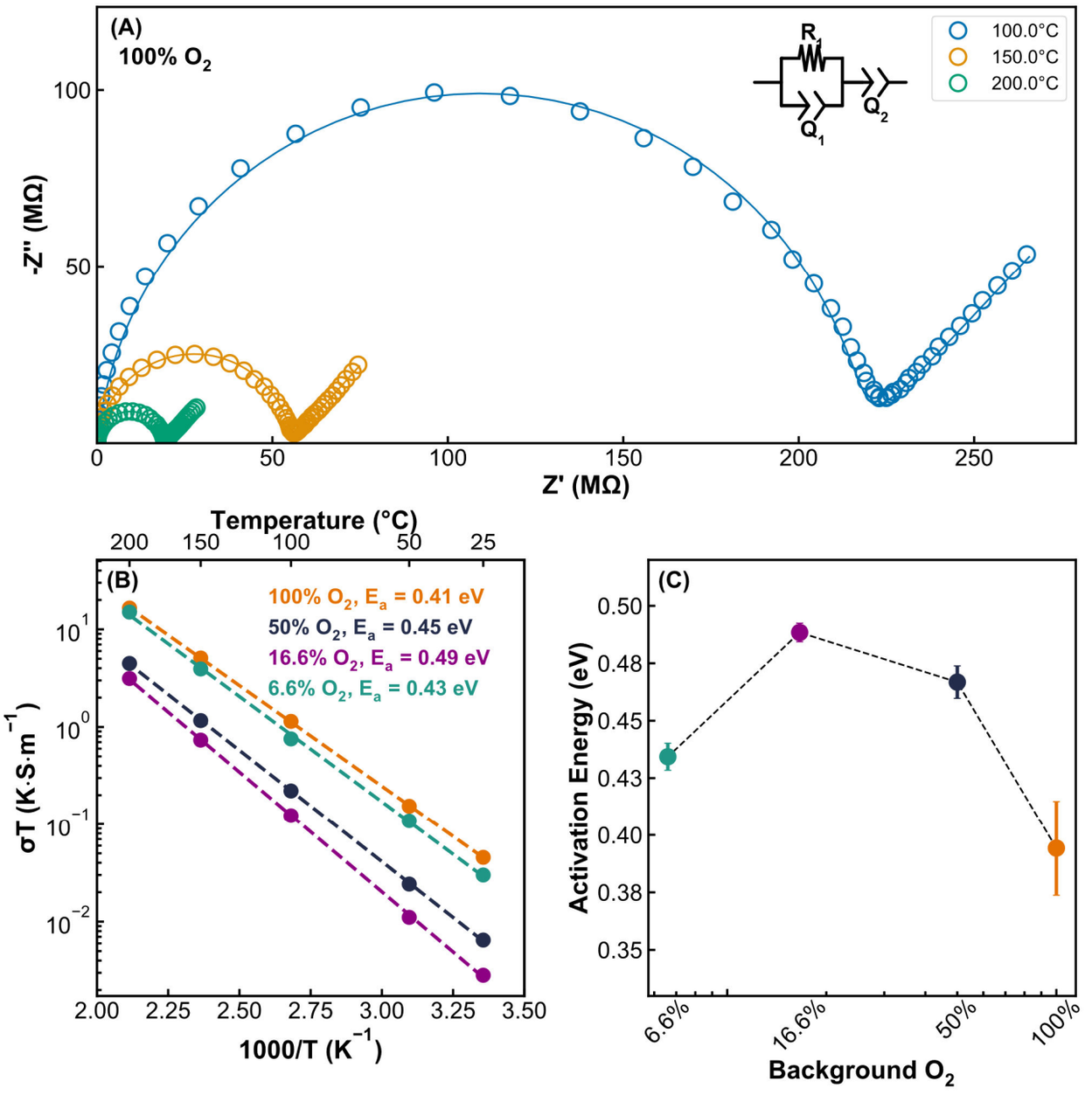

FIG. 7. (A) Representative complex plane impedance spectra measured at 100 °C, 150 °C, and 200 °C from the 100% oxygen background film. The equivalent circuit used to fit the data is shown to the left of the legend. Measured data are represented as open circles with the fit plotted as a solid line. Note that data density has been reduced to increase the legibility of the plot. (B) Arrhenius-type plot showing the dependence of conductivity on temperature. Activation energy of ion conduction values, extracted from the linear regression (dashed lines) are shown in the top right. (C) Activation energy of ion

Journal of Vacuum Science & Technology A

conduction as a function of the oxygen content of the background gas. Error bars represent the error of the linear regression fit.

IV. SUMMARY AND CONCLUSIONS

It has been shown that the partial pressure of oxygen in the background gas during PLD has a direct effect on the transfer ratio of lithium from the target to the deposited film. The amount of lithium transferred decreased monotonically with decreasing oxygen content in the background gas. It is suggested that the change in transfer ratio was driven by the replacement of oxygen in the background gas with more massive argon, which preferentially scattered the lithium in the plasma. It was also found that decreasing the oxygen content of the background gas altered the crystal structure of the films, reducing the lattice parameter for films that formed crystalline LLTaO in the as-deposited state and inhibiting the formation of LLTaO, prior to annealing, for the film prepared with 6.6% oxygen background gas. Conductivity was found to decrease with decreasing oxygen content for 100%, 50%, and 16.6% oxygen background conditions, however the conductivity increased sharply for the 6.6% oxygen background condition. The activation energy was found to vary with the inverse of the lattice parameter as a result of changes in the bottleneck size for lithium ion conduction. Changes in activation energy were ultimately determined to be the majority factor in determining the final conductivity of the films. This study provides insight into the effect of processing conditions on the structural, chemical, and ion conducting properties of lithium ion conductors and provides a platform for studying the intrinsic ion conduction properties of these materials.

ACKNOWLEDGMENTS

This work was supported by the U.S. National Science Foundation's Division of Chemical, Bioengineering, Environmental, and Transport Systems (CBET) program under award number 2055042. Utilization of the Rigaku Smartlab and Panalytical Empyrean diffractometers within the UVA Nanoscale Materials Characterization Facility

PLEASE CITE THIS ARTICLE AS DOI: 10.1116/6.0003457

Journal of Vacuum Science & Technology A

(NMCF) was fundamental to this work. This work was performed in part at the Analytical Instrumentation Facility (AIF) at North Carolina State University, which is supported by the State of North Carolina and the National Science Foundation (award number ECCS-2025064). The AIF is a member of the North Carolina Research Triangle Nanotechnology Network (RTNN), a site in the National Nanotechnology Coordinated Infrastructure (NNCI).

AUTHOR DECLARATIONS

Conflicts of Interest

The authors have no conflicts to disclose.

Author Contributions

Ian Brummel: Conceptualization (equal); Data curation (lead); Formal analysis (lead); Investigation (lead); Methodology (lead); Resources (equal); Visualization(lead); Writing – original draft (lead); Writing – review & editing (equal). **Chuanzhen Zhou:** Investigation (equal); Resources (equal); Writing – review & editing (supporting) **Jon Ihlefeld:** Conceptualization (lead); Funding acquisition (lead); Resources (lead); Supervision (lead); Writing – review & editing (equal).

DATA AVAILABILITY

The data that support the findings of this study are available from the corresponding author upon reasonable request.

Journal of Vacuum Science & Technology A

REFERENCES

[1] B.V. Lotsch and J. Maier, J. Electroceram. **38**, 128 (2017).

[2] T.K. Schwietert, V.A. Arszelewska, C. Wang, C. Yu, A. Vasileiadis, N.J.J. de Klerk, J. Hageman, T. Hupfer, I. Kerkamm, Y. Xu, E. van der Maas, E.M. Kelder, S. Ganapathy, and M. Wagemaker, Nat. Mater. **19**, 428 (2020).

[3] X. Li, J. Liang, J.T. Kim, J. Fu, H. Duan, N. Chen, R. Li, S. Zhao, J. Wang, H. Huang, and X. Sun, Adv. Mater. **34**, 2200856 (2022).

[4] C. Monroe and J. Newman, J. Electrochem. Soc. **152**, A396 (2005).

[5] T. Inoue and K. Mukai, ACS Appl. Mater. Inter. **9**, 1507 (2017).

[6] T. Famprikis, P. Canepa, J.A. Dawson, M.S. Islam, and C. Masquelier, Nat. Mater. **18**, 1278 (2019).

[7] S. Chen, K. Wen, J. Fan, Y. Bando, and D. Golberg, J. Mater. Chem. A **6**, 11631 (2018).

[8] D.B. Chrisey and G.K. Hubler, editors , *Pulsed Laser Deposition of Thin Films* (J. Wiley, New York, 1994).

[9] H.-U. Krebs, M. Weisheit, J. Faupel, E. Süske, T. Scharf, C. Fuhse, M. Störmer, K. Sturm, M. Seibt, H. Kijewski, D. Nelke, E. Panchenko, and M. Buback, "Pulsed Laser Deposition (PLD) -- A Versatile Thin Film Technique" in *Advances in Solid State Physics*, edited by B. Kramer (Springer, Berlin, Heidelberg, 2003).

[10] J.C. De Vero, G.R.S. Blanca, J.R. Vitug, W.O. Garcia, and R.V. Sarmago, Physica C **471**, 378 (2011).

[11] C. Yu, A.S. Sokolov, P. Kulik, and V.G. Harris, J. Alloy Compd. **814**, 152301 (2020).

[12] J. Schou, Appl. Surf. Sci. **255**, 5191 (2009).

[13] A. Ojeda-G-P, C.W. Schneider, M. Döbeli, T. Lippert, and A. Wokaun, Appl. Surf. Sci. **389**, 126 (2016).

Journal of Vacuum Science & Technology A

[14] L. Indrizzi, N. Ohannessian, D. Pergolesi, T. Lippert, and E. Gilardi, Helv. Chim. Acta **104**, e2000203 (2021).

[15] R. Pfenninger, M. Struzik, I. Garbayo, E. Stilp, and J.L.M. Rupp, Nat. Energy **4**, 475 (2019).

[16] J. Gonzalo, C.N. Afonso, and J. Perrière, J. Appl. Phys. **79**, 8042 (1996).

[17] H.S. Kim and H.S. Kwok, Appl. Phys. Lett. **61**, 2234 (1992).

[18] Y. Inaguma, C. Liquan, M. Itoh, T. Nakamura, T. Uchida, H. Ikuta, and M. Wakihara, Solid State Commun. **86**, 689 (1993).

[19] K. Mizumoto and S. Hayashi, Solid State Ionics **116**, 263 (1999).

[20] K. Mizumoto and S. Hayashi, J. Ceram. Soc. Jpn. **106**, 369 (1998).

[21] V. Trunov, L. Lykova, and N. Afonskii, Vestn. Mosk. U Khim.+ **9**, 55 (1968).

[22] Q. Zhou, P.J. Saines, N. Sharma, J. Ting, B.J. Kennedy, Z. Zhang, R.L. Withers, and K.S. Wallwork, Chem. Mater. **20**, 6666 (2008).

[23] I.A. Brummel, K. Wynne, W.A. Lanford, and J.F. Ihlefeld, J. Am. Ceram. Soc. **106**, 241 (2023).

[24] K. Mizumoto and S. Hayashi, J. Ceram. Soc. Jpn. **105**, 713 (1997).

[25] S. Sarkar and P. Chakraborty, Nucl. Instrum. Meth. B **212**, 364 (2003).

[26] S. Amoruso, B. Toftmann, and J. Schou, Phys. Rev. E **69**, 056403 (2004).

[27] R.B. Nuernberg, Ionics **26**, 2405 (2020).

[28] J.C. Bachman, S. Muy, A. Grimaud, H.-H. Chang, N. Pour, S.F. Lux, O. Paschos, F. Maglia, S. Lupart, P. Lamp, L. Giordano, and Y. Shao-Horn, Chem. Rev. **116**, 140 (2016).

[29] J.F. Ihlefeld, P.G. Clem, B.L. Doyle, P.G. Kotula, K.R. Fenton, and C.A. Apblett, Adv. Mater. **23**, 5663 (2011).

[30] A. Martínez-Juárez, C. Pecharromán, J.E. Iglesias, and J.M. Rojo, J. Phys. Chem. B **102**, 372 (1998).

Journal of Vacuum Science & Technology A

PLEASE CITE THIS ARTICLE AS DOI: 10.1116/6.0003457